Ranolazine inhibition of hERG potassium channels: drug-pore interactions and reduced potency against inactivation mutants

by

Chunyun Du[1 +], Yi hong Zhang[1 +], Aziza El Harchi[1], Christopher E Dempsey[2], Jules C Hancox[1, 3]

[+] **Joint first authors:** these authors contributed equally to this study

Online supplementary information

[1] School of Physiology and Pharmacology and
Cardiovascular Research Laboratories,
Medical Sciences Building,
University of Bristol,
BS8 1TD,
United Kingdom

[1] School of Biochemistry
Medical Sciences Building,
University of Bristol,
BS8 1TD,
United Kingdom

Structures of ranolazine and lidocaine

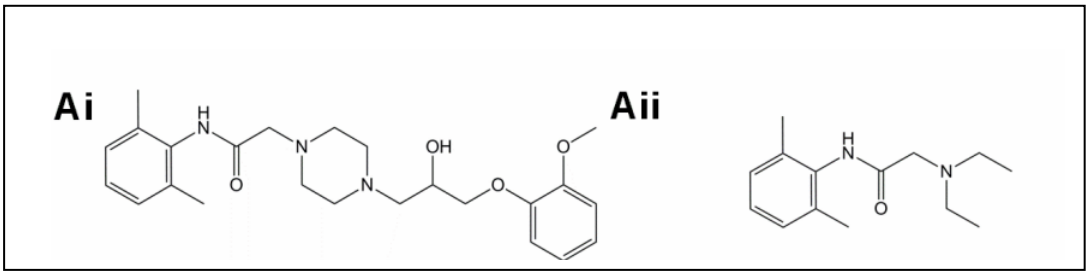

Figure S1: Chemical structures of ranolazine (Ai) and lidocaine (Aii)

Ranolazine ((+)-*N*-(2,6-dimethyphenyl0-4-[2-hydroxy-3-(2-methoxyphenoxy)-propyl]-1-piperazineacetamide) and lidocaine (2-(diethylamino)-*N*-(2,6-dimethylphenyl)acetamide) both exhibit a tertiary amine local anaesthetic (LA) structure containing hydrophobic (aromatic ring) and hydrophilic (tertiary amine) groups [1]. Recent estimates of topological surface area (TPSA) and volume for the two drugs are: TPSA 32.3 $Å^2$ for lidocaine and 74.3 $Å^2$ for ranolazine; volume 244.9 $Å^3$ for lidocaine and 411.7 $Å^3$ for ranolazine [2].

Expanded Methods and Materials

Maintenance of mammalian cell lines and cell transfection

HEK 293 cells stably expressing wild-type (WT) hERG (provided by Professor Craig January [3]) or the Y652A and F656A mutants [4] were passaged using enzyme free cell dissociation solution (Millipore, Watford, UK) and a non-enzymatic agent (Enzyme Free, Chemicon® International) and were maintained as described previously [4-7]. For transient transfection, cells were maintained as previously described [8] and were transiently transfected with cDNA plasmids (T623A, S624A and V625A hERG) using either Lipofectamine 2000 or LTX (Invitrogen, Paisley, UK) according to the manufacture's instructions. The N588K and S620T mutants were transiently transfected into Chinese Hamster Ovary cells using previously described methods. Green Fluorescent Protein (GFP, in a pCMX vector, was donated by Dr. Jeremy Tavare) [9,10] or CD8 (in pIRES, donated by Dr I Baró, University of Nantes, France) [7,8] were used as markers of successful transfection. Successfully transfected cells were identified using either green fluorescence (with excitation at 490 nm and emission at 510 nm) or Dynabeads® (Invitrogen, Paisley, UK). After transfection, the cells were incubated at 37 ^oC for a minimum of 1 day prior to any electrophysiological study.

Electrophysiological recordings

Glass coverslips onto which cells had been plated were placed in a chamber mounted on the microscope and the cells were continuously superfused at 37 ± 1 ^{o}C with standard Tyrode's solution containing (in mM): 140 NaCl, 4 KCl, 2 $CaCl_2$, 1 $MgCl_2$, 10 Glucose, 5 HEPES (titrated to pH 7.4 with NaOH). For experiments with mutants T623A and F656A and their wild-type (WT) controls, the superfusate contained 94 mM KCl (with NaCl concentration correspondingly reduced) [5,7,11]. Patch-pipettes (Corning 7052 glass, AM Systems Inc.) were pulled (Narishige, PP 830) and polished (Narishige, MF83) to give a final resistance of 2–4 MΩ. The pipette dialysis solution contained (in mM): 130 KCl, 1 $MgCl_2$, 5 EGTA, 5 MgATP; pipette pH (and thereby bulk intracellular pH) was buffered to pH 7.2 with 10 mM HEPES (titrated with KOH). Whole-cell patch-clamp recordings of membrane currents were made with an Axopatch 1D or 200B amplifier amplifier and a CV-4 1/100 head stage or a 200A or CV201 head-stage (Axon instruments). Series resistance values typically lay between 3 and 7 MΩ and were compensated by ~60–80%. Voltage-clamp commands were generated as described previously [7,8]. Data were recorded via a Digidata 1200B interface (Axon Instruments, USA) and stored on the hard-disk of a Viglen computer. A data digitization rate of 10 kHz was used during all protocols and a bandwidth of 2 kHz was set on the amplifier.

Data analysis

The fractional block of hERG $I_{tails}$was determined using an equation of the form:

$$Fractional \quad Block = 1 - \frac{I_{hERG(Drug)}}{I_{hERG(Control)}} \qquad \text{(Equation 1)}$$

Where $I_{hERG(Control)}$ is the amplitude of I_{tail} in control and $I_{hERG(Drug)}$ is the I_{tail} amplitude in the presence of the drug.

The relationship between drug concentration and I_{hERG} fractional block was determined by fitting data with a Hill-equation of the form:

$$y = \frac{1}{1 + \left(\frac{IC_{50}}{[Drug]}\right)^{h}} \qquad \text{(Equation 2)}$$

Where y is fractional block at a given concentration of Drug ([Drug]), IC_{50} is the Drug concentration producing half-maximal inhibition of I_{hERG} and *h* is the Hill coefficient for the fit to

the plotted data.

Data are presented as mean ± S.E.M. Statistical comparisons were made using paired or unpaired t tests or one/two-way analysis of variance (ANOVA).

Molecular modelling

The hERG pore model built onto the crystal structure of the bacterial K^+ channel MthK (PDB: 1LNQ; [12]) is described in detail elsewhere [7,13]. In previous docking studies we found that a modified KvAP model ("Farid model") [14] selected drug binding poses similar to those found for the MthK model. [7]. We have found that homology models built on a putative C-type inactivated state structures of the KcsA bacterial channel do not accord well with experimental data on drug-binding [15], whilst a MthK based model generally shows good concordance [15]. By contrast, although we have previously constructed a full hERG open state homology model based on a mammalian (Kv1.2/2.1 paddle chimera) template [16], this has a proline (PVP) motif that overlaps S6 residues of the canonical drug binding site (see Figure 1 in [16]). The structure of the hERG S6 helix is unlikely to be equivalent to that of the mammalian templates in this part of the pore and consequently we chose to employ bacterial channel template based models established to show good agreement with experimental drug binding data [14,15]. Docking analyses were run in parallel using both the MthK and Farid models in order to minimize model-dependence in the docking outputs and interpretations. In all models the selectivity filter contained K^+ ions in the S1 and S3 positions of the selectivity filter. K^+ ions were introduced by superimposing the selectivity filter of the high resolution KvAP structure using Insight II (Accelrys), and transferring K^+ ions into the appropriate sites of the models.

Since the crystal structures upon which the hERG pore homology models were constructed are static, we introduced pore model flexibility by allowing free side chain bond rotation for residues in or near the bottom of the selectivity filter (T623, S624 and V625) and for residues that project from the S6 helices towards the pore cavity (Y652, F656, S660). Free conformational sampling around all rotatable bonds in the drug molecules was allowed. In each docking run 60,000 generations of the Genetic Algorithm were run; to increase sampling of configurational space each docking run of each drug into each model was repeated 240 times using different starting configurations with the drug repositioned and reoriented in the pore cavity.

In a set of runs made to explore possible binding of drugs near S620, the drug binding cavity was

redefined to include S620 and all residues within 10 Å and an appropriate set of new residue beside chain bond rotations (including S620) was sampled. Since Flexidock was unable to find low energy score docked poses involving direct interaction of drugs with S620, these results are not shown here.

Supplementary Results

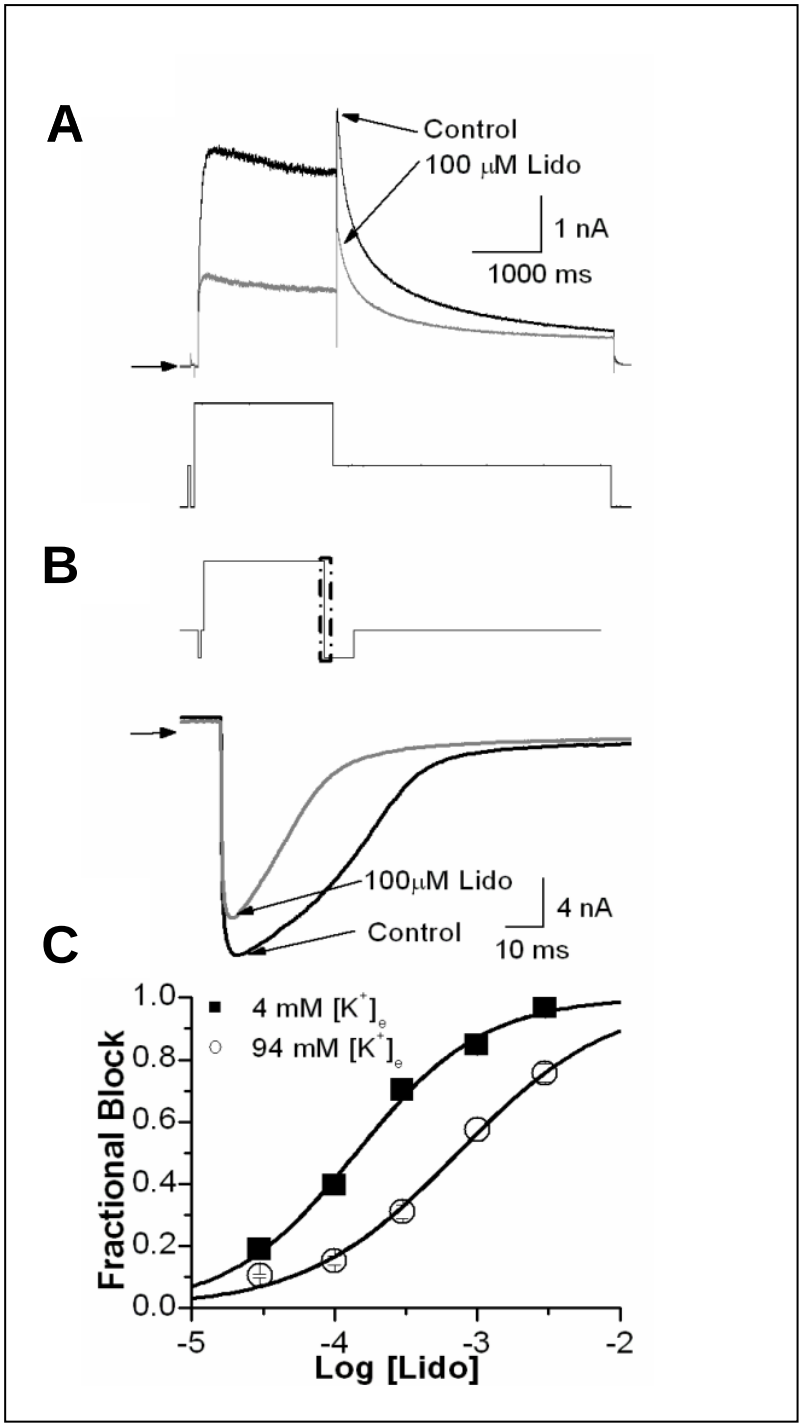

.

Figure S2: **Block of WT I_{hERG} by lidocaine**
(A) Effects of lidocaine studied using the same standard I_{hERG} pharmacology protocol (described in the main text, and shown above as the lower trace in A) as used for ranolazine. Upper traces in A show WT I_{hERG} elicited in Control solution and in the presence of 100 μM lidocaine.
(B) Upper trace shows voltage protocol used to elicit WT I_{hERG} in 94 mM $[K^+]_e$. Boxed area shows repolarizing phase of protocol from +20 to -120 mV. Lower trace shows WT I_{hERG} records on repolarization to -120 mV in Control and in 100 μM lidocaine.
Horizontal arrows in A and B denote zero current. The brief (50 ms) steps to -40 mV and -120 mV

in A and B respectively elicited reference (nominally hERG-free) current against which peak outward/inward I_{hERG} was measured.
(C) shows concentration-response relations for inhibition of WT I_{hERG} by lidocaine in 4 mM $[K^+]_e$ (filled squares) and in 94 mM $[K^+]_e$ (open circles). Data were fitted with a Hill-equation. Note that error bars for some points are small and are obscured by the symbols ($n \geq 5$ cells per data-point).

Figure S2 shows results from similar experiments performed using lidocaine to those shown in Figure 1 (main paper text) on ranolazine. Figure S2A shows representative control and lidocaine (100 μM) traces in normal (4mM) $[K^+]_e$. Four lidocaine concentrations were studied, mean fractional block for each concentration then calculated and a concentration-response relation constructed as shown in Figure S2C (filled squares). The derived IC_{50} was 141.77 ± 9.81 μM (h=0.98 ± 0.07). Figure S2B shows the protocol used and representative traces obtained in determining the effect of 100 μM lidocaine on inward I_{hERG} elicited in 94 mM $[K^+]_e$. Again four concentrations were tested, mean fractional block at each concentration calculated and a concentration-response relation constructed (Figure S2C open circles). The derived IC_{50} for inward I_{hERG} in high $[K^+]_e$ of 735.32±54.03 μM (h = 0.82 ± 0.05). In principle, reduced inward I_{hERG} block with raised $[K^+]_e$ could arise from attenuation of inactivation with raised $[K^+]_e$ or the alteration of direction of K^+ ion flux [17]. Therefore the effects of lidocaine on inward I_{hERG} in standard (4 mM) $[K^+]_e$ were also studied (data not shown), yielding an IC_{50} value of 588.96 ± 110.28 μM (h = 0.77 ±0.13). Thus, the reduced lidocaine block with inward K^+ flux was largely retained with a normal $[K^+]_e$, suggestive of a direct interaction between the permeant ion and the drug.

Effect of ranolazine on voltage-dependence of WT I_{hERG}

The voltage-dependence of I_{hERG} inhibition by ranolazine was determined using the protocol shown in lower panels of Figures S3A and B (comprised of 2s steps to different test potentials, followed by repolarization to -40 mV to elicit current tails; I_{tail}). Successive command pulses were applied at 12-second intervals. The protocol was applied in control and during superfusion with ranolazine-containing solutions. Figure S3 A and B show example WT I_{hERG} current traces recorded from the same cell in the absence (A) and presence (B) of 10 μM ranolazine. I_{hERG} amplitude both during depolarizing steps and on repolarization was reduced when cells were exposed to 10 μM ranolazine (Figure S3B). In order to determine ranolazine inhibition of I_{hERG} at different voltages, I_{hERG} amplitude at the end of the depolarization step was measured and the I-V relationship was constructed as shown in Figure S3C. For each cell and each condition (control,

drug) current amplitude was normalized to the maximal control current during the protocol. The I-V relationship showed a characteristic bell-shaped appearance both in control and in the presence of 10 µM ranolazine. I_{hERG} amplitude was smaller in the presence of ranolazine between voltages from -20 to +60 mV (indicated by symbols above points on Figure 6.4 C, two-way ANOVA followed by a Bonferroni post-test, n= 6 cells).

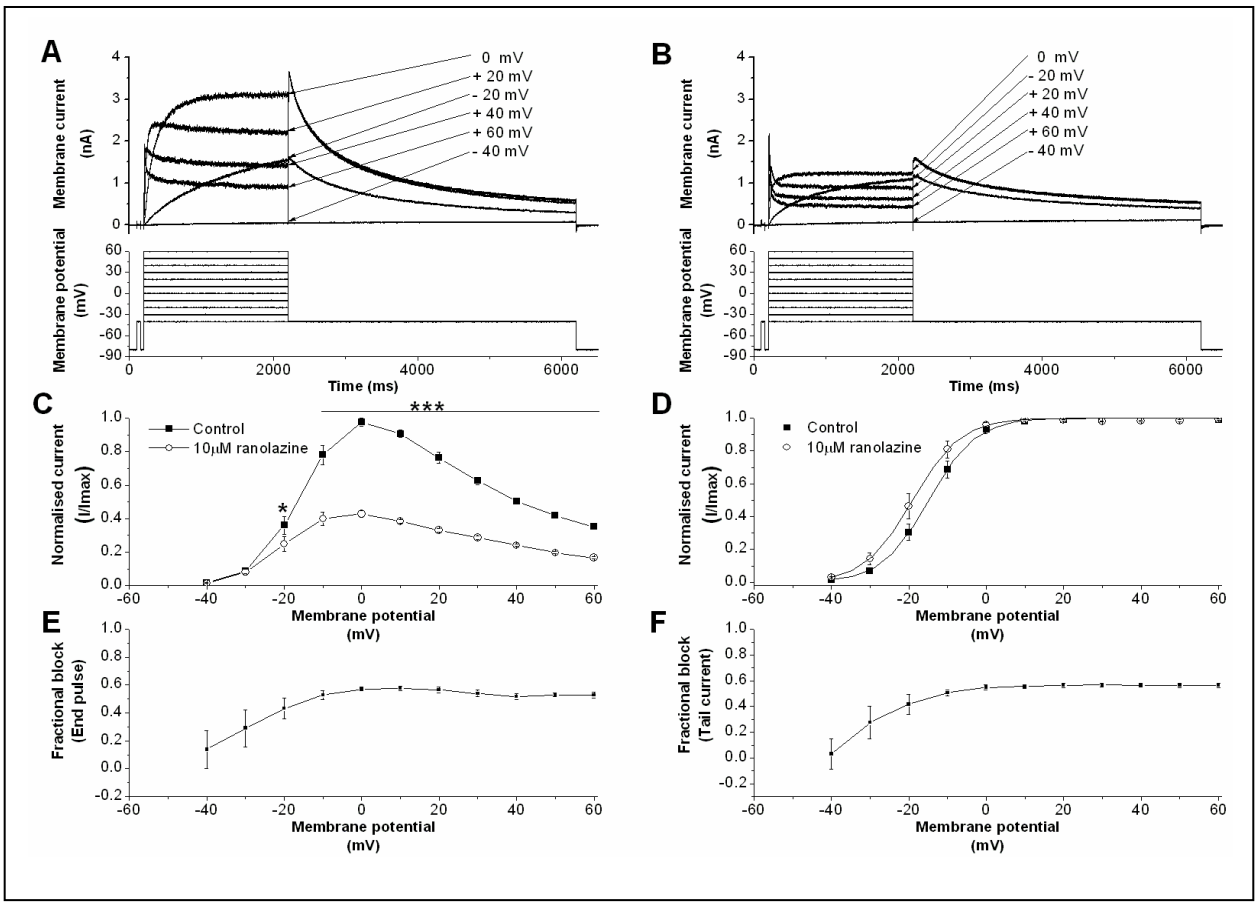

Figure S3 Effect of ranolazine on the voltage-dependence of I_{hERG}

(A, B). Representative families of I_{hERG} in the absence (A) and presence (B) of 10 µM ranolazine elicited by the voltage protocol shown in lower panels (same protocol as shown in Figure 3.3). Some current traces are omitted for clarity of display.

(C) I-V relations for end-pulse current with and without 10 µM ranolazine (n= 6 cells). Data were normalised to the maximal I_{hERG} current during the protocol and then plotted against test potentials.

(D) Steady-state activation plots for I_{hERG} derived from tail current measurements on repolarization to -40 mV in the absence and presence of 10 µM ranolazine. The I_{tails} were normalised to the maximal tail current recorded during the protocol and then plotted against test potential.

(E) Plot of mean (±SEM) fractional block of I_{hERG} against test voltage for end-pulse current (n = 6 cells).

(F) Plot of mean (±SEM) fractional block of I_{hERG} tails against test voltage (n = 6 cells).

Note that error bars for some of the points are small and are obscured by the symbols.

"*" denotes statistical significance of $p<0.05$; "***" denotes statistical significance of $p<0.001$; (2-way ANOVA followed by a Bonferroni post-test).

The voltage-dependence of I_{hERG} activation was evaluated by plotting normalised I-V relations for the hERG I_{tails} (with I_{tail} at each voltage in each condition normalized to the maximal I_{tail} amplitude during the protocol) and is shown in Figure S3D: for currents in both control and ranolazine, I_{tail} amplitude increased with depolarization to more positive potentials, reaching a plateau at ~ +10 mV. The data were fitted with a standard Boltzmann function to give a $V_{0.5}$ of -14.80 ±1.39 mV in control (k= 5.72 ±0.32 mV) and a $V_{0.5}$ of -18.95 ±1.87 mV (k= 5.53 ±0.14 mV) with 10 μM of ranolazine (p< 0.05, paired t-test; n= 6 cells). Thus the voltage-dependence of I_{hERG} activation was negatively shifted by ranolazine. Voltage-dependence of current inhibition by ranolazine was also assessed and is shown in Figure S3 E and F. One-way ANOVA analysis showed inhibition to be voltage-dependent for both end-pulse and tail currents (p<0.05). For the I_{end} plots, the fractional inhibition at -40 mV was significantly smaller than at other voltages; whilst for I_{tail} plots, those blocking values at -40 and -30 mV were significantly smaller than at other voltages. There was no significant difference in fractional block over the potential range between -20 mV and +60 mV for either end-pulse or tail current (n= 6 cells; one-way ANOVA, followed by Bonferroni post-test).

These findings are consistent with those of Rajamani and colleagues [18], who also found I_{hERG} inhibition by ranolazine during step protocols to show voltage dependence and observed a left-ward shift in voltage-dependent activation (by ~-7 mV with 30 μM ranolazine; compared to ~-4 mV with 10 μM ranolazine in the present study).

Effect of the S620T hERG mutation on the action of lidocaine

For comparison with ranolazine, further experiments were performed in which the effects of the S620T mutation on lidocaine block of I_{hERG} were examined. The same voltage protocol was used as used for both the WT I_{hERG} concentration-response data and to study effects of S620T on ranolazine block of I_{hERG}. Figure S4A shows the effect of a high (1mM) concentration of lidocaine on S620T I_{hERG}. Only modest I_{hERG} inhibition was produced by this lidocaine concentration (which produced >80% inhibition of WT I_{hERG}). Figure S4B shows the concentration-response relation for S620T I_{hERG} inhibition, also displayed in the same plot is the corresponding relation for WT $I_{hERG.}$ The derived IC_{50} for lidocaine inhibition of S620T was 6880 ± 1110 μM (h= 0.51 ± 0.05), which is ~49-fold its WT control.

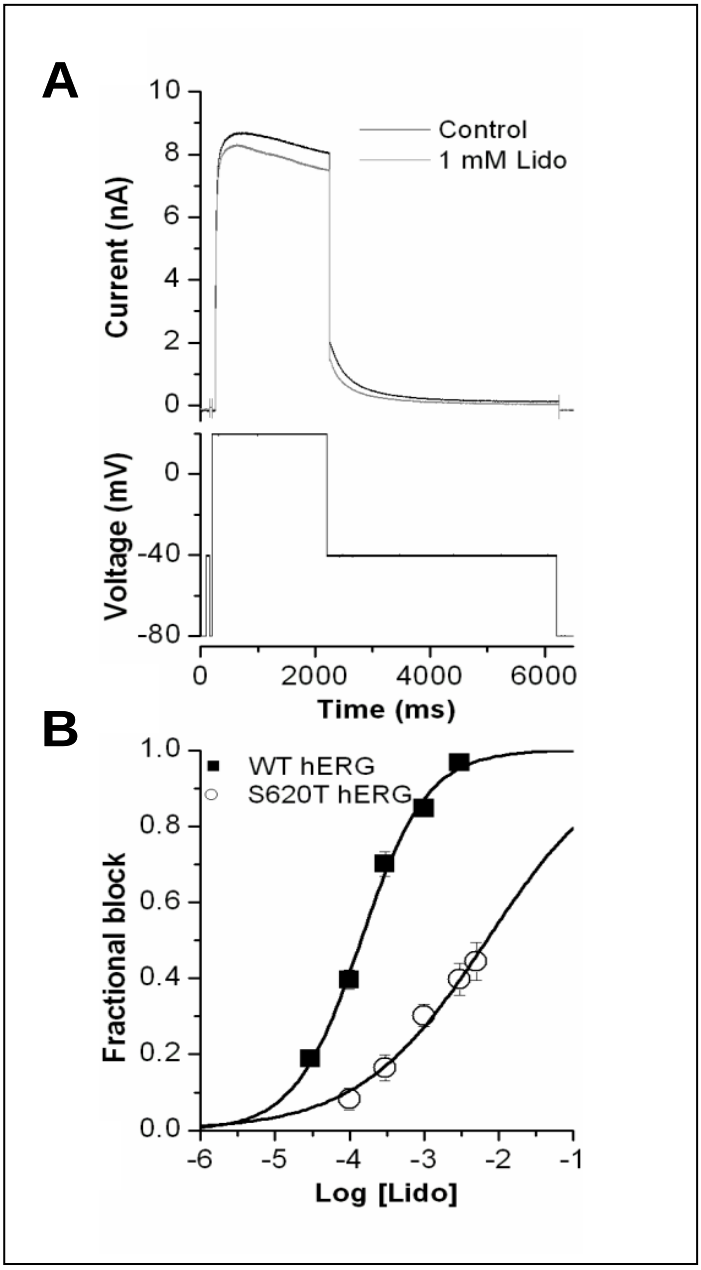

Figure S4: Effect of the S620T mutation on I_{hERG} inhibition by lidocaine.

A. Upper traces show representative currents for S620T I_{hERG} in control solution and following exposure to 1mM lidocaine elicited by the voltage protocol shown below the current records
B. Concentration response relation for S620T I_{hERG} inhibition compared with that for WT I_{hERG} obtained with the same voltage protocol. IC_{50} and *h* values are given in the text. n ≥ 5 cells per data-point.

Docking of lidocaine and ranolazine to hERG Y652A and F656A mutant channels

The suppression of lidocaine block of I_{hERG} by the F656A and Y652A mutations (main text Figures 3Bii and 3Dii) was very small, indicating that neither of these side chains is essential for block. To assess whether these observations can be understood in terms of a degeneracy/redundancy in potential binding partners for the lidocaine aromatic group we docked the drug into hERG pore models carrying *either* the Y652A or F656A mutation (Figure S5). These runs showed that low energy score poses can be obtained with the tertiary amino group positioned near the pore cavity K^+ binding site, and the lidocaine aromatic group making interactions with either F656 or Y652 (Figure S5). Thus it was possible for lidocaine block to be maintained in Y652A and F656A mutants because the lidocaine aromatic ring was able to make interactions with either a Y652 (in the case of F656A) or a F656 (in the case of Y652A) aromatic side chain.

In the case of ranolazine, both Y652A and F656A mutations resulted in a loss of aromatic interactions involving one of the aromatic groups on the drug (Figure S6), consistent with the large decreases in affinity for block of each of these mutant channels (main text Figures 3Bi and 3Di). Unlike lidocaine, interactions with *both* Y652 and F656 aromatic side chains are required to express full hERG block by ranolazine.

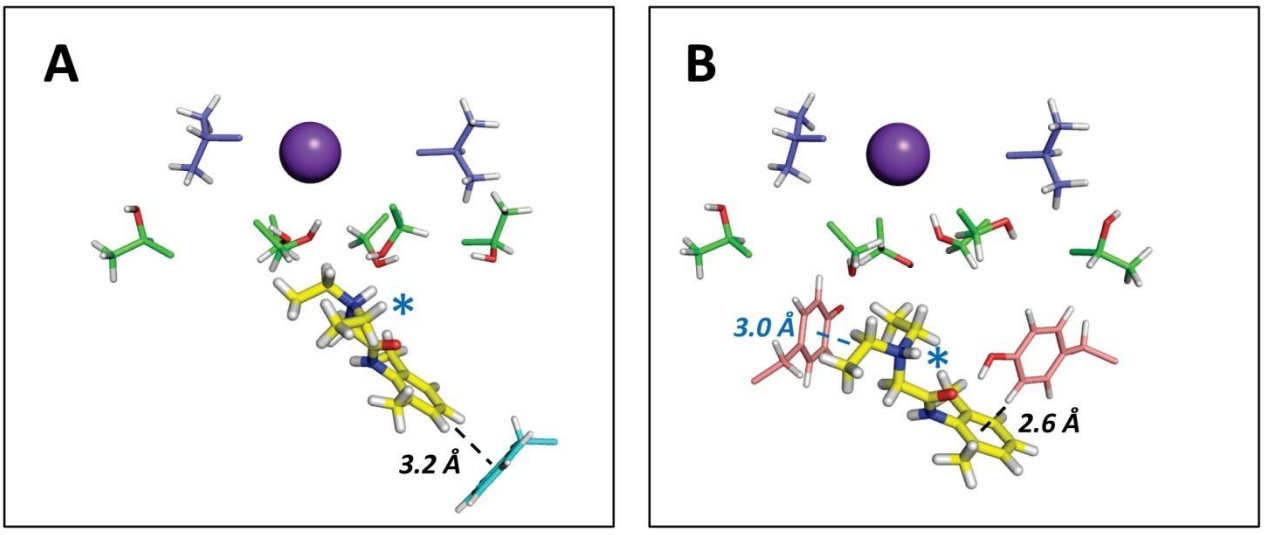

Figure S5: Representative low energy score docking poses for lidocaine (yellow stick representation) in the MthK hERG pore model containing the Y652A mutation (A) or F656A mutation (B). hERG pore side chains are V625 (dark blue), T623 and S624 (green), Y652 (salmon) and F656 (light blue). Side chains of Y652 and F656 are shown only if they make aromatic or cation-π interactions with lidocaine. The blue star indicates the location of the tertiary amino group

of lidocaine.

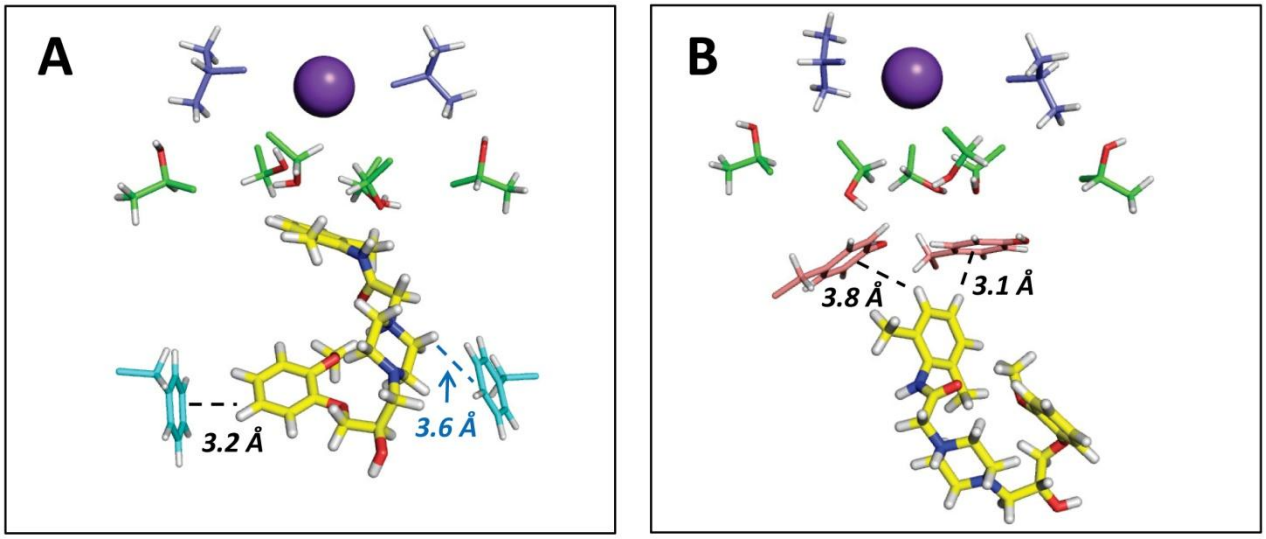

Figure S6: Representative low energy score docking poses for ranolazine in the MthK hERG pore model containing the Y652A mutation (A) or F656A mutation (B). The residue colors and annotations are as described in the legend to Figure S5.

Potency of hERG blockers with inactivated-state preference scales with the number of interactions between drug and hERG pore residues

We recently showed that the IC_{50} values of hERG blockers with blocking affinity enhanced by inactivation was related to the number of defined interactions each drug made with amino acid residues in the MthK-based hERG pore model used here [15]. Ranolazine and lidocaine conform to this relationship (Figure S7) supporting the interpretation that the enhanced binding of ranolazine in the hERG pore cavity compared to lidocaine results from the larger number of interactions possible with the larger drug compared to the smaller one. In this analysis the number of defined interactions between drug and hERG pore residues was averaged over the 5 lowest energy score docked outputs for each drug. Defined interactions comprise hydrogen bonds, cation-π and π–π interactions between aromatic rings, and the location of the protonated aliphatic amino group near the cavity binding site of a K^+ ion in high resolution structures of homologous ion channels as indicated in Figures 5, S5 and S6. The distance criteria for these interactions are defined in reference 15.

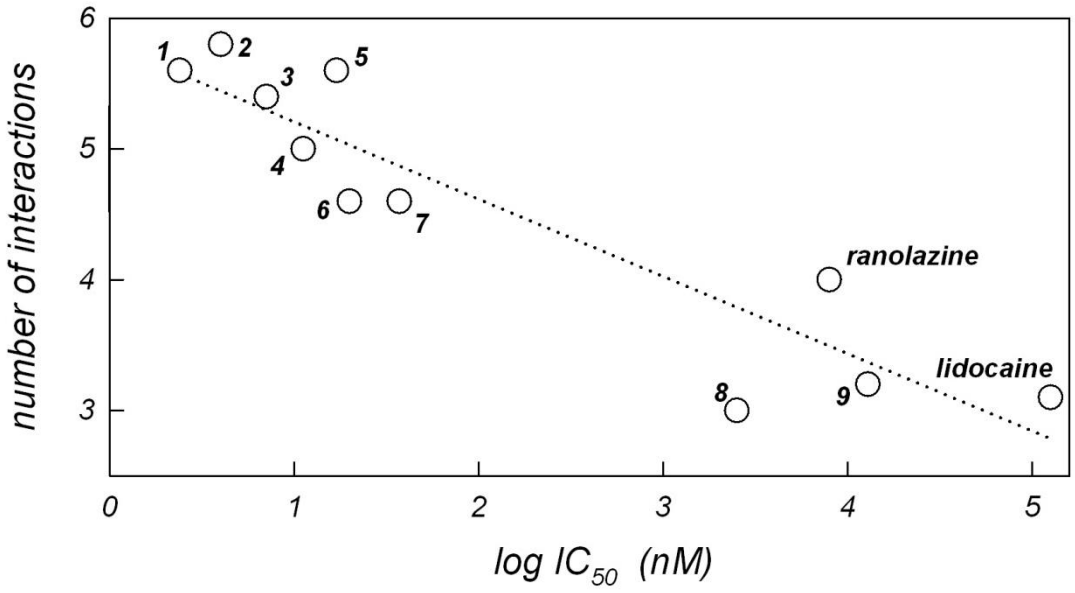

Figure S7: Relationship between hERG block potency (log IC_{50}) and number of interactions with hERG pore residues for hERG blockers including ranolazine and lidocaine measured in low energy score docking outputs from the MthK model using FlexiDock. The numbered hERG blockers are: 1, cavalli-6; 2, dofetilide; 3, terfenadine; 4, E-4031; 5, cavalli-2; 6, cisapride; 7, haloperidol; 8, chloroquine; 9, S-bupivacaine. See reference 15 for further details.

Summary tables of effects of hERG mutations on I_{hERG} inhibition by ranolazine and lidocaine

Table S1: Ranolazine inhibition of WT and mutant hERG channels

Channel	Repolarization step	K^+	Concentration range	IC_{50} (mean ± sem)	*h* value (mean ± sem)	Shift in potency -compared to its WT-Control
	mV	mM	µM	µM		
WT-1	-40	4	0.3-100	8.03 ± 0.95	0.8 1± 0.07	
WT-2	-120	94	0.1- 100	8.47 ± 2.63	0.58 ± 0.1	1.05
S620T	-40	4	10-800	582.65 ± 23.36	0.89 ± 0.05	72.56
T623A	-120	94	10-500	159.21 ± 2.42	0.52 ± 0.006	18.80
S624A	-40	4	1-100	61.53 ± 12.93	0.93 ± 0.19	7.66
V625A	-120	4	1-300	63.14 ± 6.88	0.58 ± 0.04	7.86
Y652A	-40	4	10-500	173.62 ± 39.73	0.64 ± 0.14	21.62
F656A	-120	94	10-500	452.67 ± 12.07	0.68 ± 0.02	53.44
N588K	-40	4	10-300	124.08 ± 7.39	0.81 ± 0.05	15.45

Table S2: Lidocaine inhibition of WT and mutant hERG channels

Channel	Repolarization step	K^+	Concentration range	IC_{50} (mean ± sem)	*h* value (mean ± sem)	Shift in potency - compared to its WT-Control
	mV	mM	µM	µM		
WT-1	-40	4	30-3000	141.77±9.81	0.98±0.07	
WT-2	-120	4	30-3000	588.96±110.28	0.77±0.13	4.15
WT-3	-120	94	30-3000	735.32±54.03	0.82±0.05	5.19
S620T	-40	4	100-5000	6880±1110	0.51±0.05	48.53
T623A	-120	94	100-3000	746.48±70.40	0.81±0.07	1.01
S624A	-40	4	30-1000	107.59±14.18	1.03±0.14	0.76
V625A	-120	4	30-3000	1580.0±75.48	0.51±0.01	2.68
Y652A	-40	4	100-3000	544.33±34.03	0.95±0.06	3.84
F656A	-120	94	100-3000	848.12±65.54	0.85±0.06	1.15

These summary tables show IC_{50} values for WT I_{hERG} tails using the standard +20 mV protocol, with I_{tail} measured at -40 mV and for measurements at -120 mV in high $[K^+]_e$. Comparable summary data are then shown for the mutant hERG channels studied. The right-most column shows fold-changes in IC_{50} with each mutant compared to their relevant WT control, or for WT measurements with WT-1

References

[1] Fredj S, Sampson KJ, Liu H, Kass RS. Molecular basis of ranolazine block of LQT-3 mutant sodium channels: evidence for site of action. Br J Pharmacol 2006;148:16-24.

[2] Pless SA, Galpin JD, Frankel A, Ahern CA. Molecular basis for class Ib anti-arrhythmic inhibition of cardiac sodium channels. Nat Commun 2011;2:351 doi: 10.1038/ncomms1351.

[3] Zhou Z, Gong Q, Ye B, Fan Z, Makielski JC, Robertson GA et al. Properties of HERG channels stably expressed in HEK 293 cells studied at physiological temperature. Biophys J 1998;74:230-41.

[4] Milnes JT, Crociani O, Arcangeli A, Hancox JC, Witchel HJ. Blockade of HERG potassium currents by fluvoxamine: incomplete attenuation by S6 mutations at F656 or Y652. Br J Pharmacol 2003;139:887-98.

[5] Ridley JM, Dooley PC, Milnes JT, Witchel HJ, Hancox JC. Lidoflazine is a high affinity blocker of the HERG K^+ channel. J Mol Cell Cardiol 2004;36:701-5.

[6] Ridley JM, Milnes JT, Zhang YH, Witchel HJ, Hancox JC. Inhibition of HERG K^+ current and prolongation of the guinea-pig ventricular action potential by 4-aminopyridine. J Physiol 2003;549:667-72.

[7] El Harchi A, Zhang YH, Hussein L, Dempsey CE, Hancox JC. Molecular determinants of hERG potassium channel inhibition by disopyramide. J Mol Cell Cardiol 2012;52:185-95.

[8] Zhang YH, Colenso CK, Sessions RB, Dempsey CE, Hancox JC. The hERG K^+ channel S4 domain L532P mutation: characterization at 37 degrees C. Biochim Biophys Acta 2011;1808:2477-87.

[9] McPate MJ, Zhang H, Ideniran I, Cordeiro JM, Witchel HJ, Hancox JC. Comparative effects of the short QT N588K mutation at 37^{o}C on hERG K^+ channel current during ventricular, Purkinje fibre and atrial action potentials: an action potential clamp study. J Physiol Pharmacol 2009;60:23-41.

[10] Du CY, El Harchi A, McPate MJ, Orchard CH, Hancox JC. Enhanced inhibitory effect of acidosis on hERG potassium channels that incorporate the hERG1b isoform. Biochem Biophys Res Commun 2011;405:222-7.

[11] Ridley JM, Milnes JT, Witchel HJ, Hancox JC. High affinity HERG K^+ channel blockade by the antiarrhythmic agent dronedarone: resistance to mutations of the S6 residues Y652 and F656. Biochem Biophys Res Comm 2004;325:883-91.

[12] Jiang Y, Lee A, Chen J, Cadene M, Chait BT, MacKinnon R. Crystal structure and mechanism of a calcium-gated potassium channel. Nature 2002;417:515-22.

[13] Witchel HJ, Dempsey CE, Sessions RB, Perry M, Milnes JT, Hancox JC et al. The low-potency, voltage-dependent HERG channel blocker propafenone - molecular determinants and drug trapping. Mol Pharmacol 2004;66:1201-12.

[14] Farid R, Day T, Friesner RA, Pearlstein RA. New insights about HERG blockade obtained from protein modeling, potential energy mapping, and docking studies. *Bioorg Med Chem* 2006;14:3160-73.

[15] Dempsey CE, Wright D, Colenso CK, Sessions RB, Hancox JC. Assessing HERG pore models as templates for drug docking using published experimental constraints: the inactivated state in the context of drug block. J Chem Inf Model 2014;54:601-12.

[16] Colenso CK, Sessions RB, Zhang YH, Hancox JC, Dempsey CE. Interactions between voltage sensor and pore domains in a hERG K^+ channel model from molecular simulations and the effects of a voltage sensor mutation. J Chem Inf Model 2014;53:1358-1370.

[17] Yang T, Roden DM. Extracellular potassium modulation of drug block of I_{Kr}. Implications for torsade de pointes and reverse use-dependence. Circulation 1996;93:407-11.

[18] Rajamani S, Shryock JC, Belardinelli L. Rapid kinetic interactions of ranolazine with HERG K^+ current. J Cardiovasc Pharmacol 2008;51:581-9.